

Fabrication and mechanical characterization of long and different penetrating length neural microelectrode arrays

This content has been downloaded from IOPscience. Please scroll down to see the full text.

2015 J. Micromech. Microeng. 25 055014

(<http://iopscience.iop.org/0960-1317/25/5/055014>)

View [the table of contents for this issue](#), or go to the [journal homepage](#) for more

Download details:

IP Address: 193.137.10.167

This content was downloaded on 05/06/2015 at 07:45

Please note that [terms and conditions apply](#).

Fabrication and mechanical characterization of long and different penetrating length neural microelectrode arrays

S B Goncalves¹, A C Peixoto¹, A F Silva² and J H Correia¹

¹ Department of Industrial Electronics, University of Minho, Guimaraes, Portugal

² MIT Portugal Program, School of Engineering, University of Minho, Guimaraes, Portugal

E-mail: sgoncalves@dei.uminho.pt

Received 6 July 2014, revised 29 August 2014

Accepted for publication 2 September 2014

Published 17 April 2015



Abstract

This paper presents a detailed description of the design, fabrication and mechanical characterization of 3D microelectrode arrays (MEA) that comprise high aspect-ratio shafts and different penetrating lengths of electrodes (from 3 mm to 4 mm). The array's design relies only on a bulk silicon substrate dicing saw technology. The encapsulation process is accomplished by a medical epoxy resin and platinum is used as the transduction layer between the probe and neural tissue. The probe's mechanical behaviour can significantly affect the neural tissue during implantation time. Thus, we measured the MEA maximum insertion force in an agar gel phantom and a porcine cadaver brain. Successful 3D MEA were produced with shafts of 3 mm, 3.5 mm and 4 mm in length. At a speed of 180 mm min⁻¹, the MEA show maximum penetrating forces per electrode of 2.65 mN and 12.5 mN for agar and brain tissue, respectively. A simple and reproducible fabrication method was demonstrated, capable of producing longer penetrating shafts than previously reported arrays using the same fabrication technology. Furthermore, shafts with sharp tips were achieved in the fabrication process simply by using a V-shaped blade.

Keywords: neural electrodes, dicing technology, mechanical characterization

(Some figures may appear in colour only in the online journal)

1. Introduction

Invasive neural interfaces capable of communication with neural tissue are emergent therapeutics. This approach relies on electrodes implanted inside the brain, restoring lost neural function by recording and/or electrically stimulating a large number of small groups of neurons. Deep brain stimulation (DBS) has proved to have beneficial effects in a variety of neurological conditions, such as Parkinson's disease, essential tremor, dystonia, Tourette's syndrome, chronic pain, epilepsy, depression and obsessive compulsive disorder (OCD) [1, 2]. Cochlear [3] and retinal [4] implants are also widely used in the therapy of deafness and blindness, respectively. More recently, studies have been trying to achieve control of artificial limbs through implantable electrodes [5, 6].

Current fabrication methods of 3D microprobe array structures can be divided into three principal branches: silicon bulk etched microprobe array; polymer-constructed array; and 3D arrays assembled from 2D parts [7]. Three dimensional microelectrode arrays (MEA) based on silicon technologies are receiving a growing amount of interest, since they enable a pronounced increase in the number of recording sites per probe shaft [8]. Two well-known silicon-based configurations of invasive neural microelectrodes are the Michigan probe and the Utah Electrode Array (UEA), which are nowadays still the reference point to several studies [9, 10]. The Michigan configuration includes single-shaft, multi-shaft and 3D layouts with multiple recording sites per electrode [10]. On the other hand, the UEA configuration comprises a 3D array of one hundred needle-shaped microelectrodes and each shaft has an

Table 1. Comparison of design parameters between some silicon-based 3D MEA.

Reference	Array dimension	Array fabrication method	Number of electrodes per shaft	Number of shafts	Length (mm)	Width (μm)	Thickness(μm)
[8]	2D	Dry silicon etching process	9	1, 4	8	140	100
[14]			3	4	10	100	50
[15]			8	4, 8	7–8	—	—
[16]			188	1, 4	4	180	300
[20]			16 (8×8)	2	5	190	50
[7]	3D array by 2D parts assembly	Silicon micromachining	4	16 (4×4)	6	100	250
[17]		1	128 (8×16)	1–2.5	40	15	
[18]		1	16 (4×4)	1.2	50	12	
[19]		8	32 (4×8)	3.3	144	80	
[21]		5	16 (4×4)	2, 4.5, 8	140	100	
[22]		4	16 (4×4)	4	60	—	
[25]	3D	Wet-etching	4	4 (2×2)	4	200	30
[24]	array	μ -WEDM ^a	1	100 (10×10)	5, 9	200	200

active tip that communicates with the neural tissue. Currently, UEA electrodes have a maximum length of 1.5 mm, which restricts their application to surface structures of the cerebral cortex [11–13].

The desire to increase scientific insight into the interaction of neuron populations has triggered the need for longer penetrating electrodes. Therefore, in the last decade several approaches based on different technologies were developed to produce invasive neural interfaces with deeper electrode shafts. Most of these approaches include planar microfabricated 2D MEA [8, 14–16] or 3D structures that are assembled by layers of 2D arrays [7, 17–22]. However, both approaches have disadvantages, when compared to technologies that simply rely on silicon wafer micromachining like the UEA array [23].

Planar electrodes have an inherent 2D nature, recording along a single plane of the brain, which prevents the full neurons and cell activity information in 3D space. On the other hand, 3D MEA ensure the simultaneous monitoring and stimulation of neural activity within a targeted volume of brain tissue with a high spatial resolution. This allows for more realistic and complete information of neural networks. Although 3D arrays resulting from assembly techniques are capable of performing as 3D interfaces, they have some drawbacks. They require complex assembly steps and vertical interconnection to produce 3D structures. Besides this, they have a low structure strength and a large implantable opening [7]. Multiple active sites along the shafts are easily achieved.

Some efforts have been made to obtain 3D MEA with long electrodes based on silicon wafers micromachining which also include microwire electrical discharge machining [24] and self-assembled probes using a heat treatment processes [25] to achieve the final 3D array design. We have previously presented [26] an approach to fabricate 3D MEA with shaft lengths up to 3 mm, which use aluminum as the bulk material instead of silicon. Table 1 compares the 3D MEA with regard to their design parameters.

In this paper we will focus on technologies that rely on wafer dicing to define the 3D array and to achieve longer electrode shafts. The final 6×6 matrix comprises three different

lengths for the shafts, the longest being 4 mm and the shortest 3 mm. The fabrication process is characterized by its simplicity, low-cost and reproducibility. Since depths of up to 4 mm are reached, the proposed electrode matrix enables the recording/stimulation of deeper neural structures than the cerebral cortex, such as a rat's hippocampus. This neural structure is a frequently used research model for exploring both normal and pathological conditions of the nervous system, including the processes involved in memory and learning as well as neurodegenerative diseases [27].

Mechanical characterization of the final array was also performed using a 0.5% agar gel phantom and a porcine cadaver brain, in order to measure the MEA's maximum insertion and withdrawal forces. Mechanical characterization of arrays is essential, since some of the leading hypotheses for the failure of neuroprosthesis relate to acute injury caused by insertion [28].

2. MEA design

The developed neural MEA consists of 36 sharp electrode probes fabricated on a silicon substrate. The structure comprises three different electrode lengths: 3 mm, 3.5 mm and 4 mm. Its structure is divided into three regions: a support base region, the electrode body (shaft) and a piercing region (sharp tip) that is simultaneously the recording/stimulating region, as shown in figure 1(a). The square support base region measures $3.45 \times 3.45 \text{ mm}^2$ and the electrode's shaft is $150 \mu\text{m}$ wide. The base region is supported by an epoxy filling, which also allows interelectrode electrical isolation. The wide electrode shaft is designed to be robust enough to withstand implantation. After the insulation process of the array, each shaft ends up with a width of $180 \mu\text{m}$ along the electrode length. The sharp tip at the shaft's end corresponds to a recording/stimulating region which is covered by a titanium (Ti) and platinum (Pt) layer. Ti serves as the adhesion promoter for the Pt thin film, which is the material that interfaces with the neural tissue. Pt was selected due to its biocompatibility and impedance characteristics [29]. The

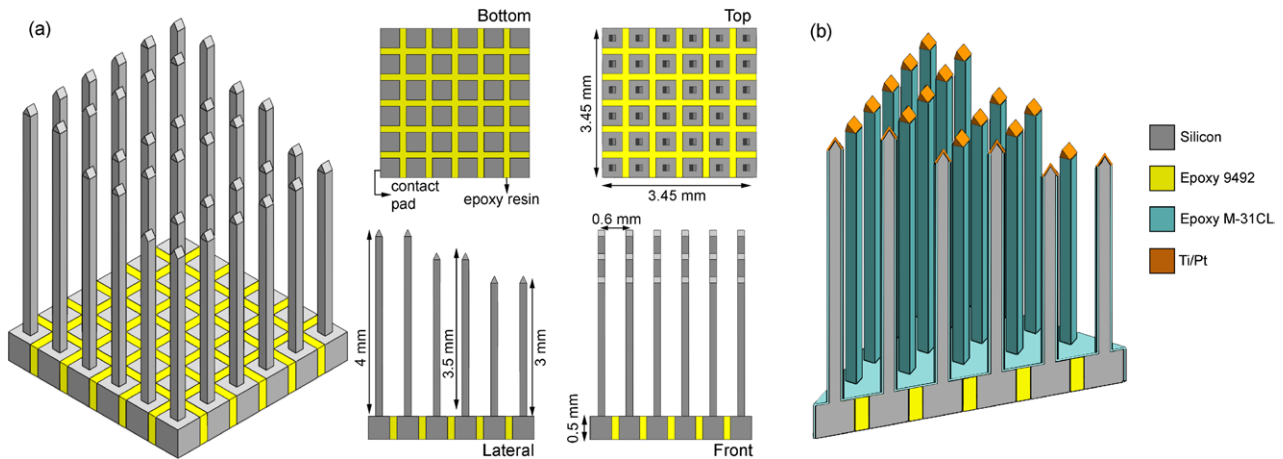


Figure 1. (a) 3D schematic of the MEA after the dicing saw process to create the array design. At this step of the fabrication process the high-aspect-ratio and different penetrating lengths of electrodes can be seen; (b) transversal cut of the 3D final array showing the insulation and transduction layers.

electrode tips are placed $600\ \mu\text{m}$ from each other. Figure 1(b) shows the schematic of the final 3D MEA design.

3. Fabrication process

Figure 2 illustrates the process flow of the 3D MEA fabrication, whose design is exclusively accomplished by a dicing saw that patterns the silicon substrate. The cutting stages are performed on a Disco DAD 2H/6T dicing machine, equipped with a Disco NBC-ZB diamond grit blade capable of performing cuts 4 mm deep and $150\ \mu\text{m}$ wide at a cutting speed of $0.3\ \text{mm s}^{-1}$. Some modifications had to be made in the way the dicing machine performs the Z-axis calibration in order to cut samples that are higher than the 2 mm limit of the machine. By placing an aluminum spacer between the blade and the sample holder, it is possible to cut at heights up to 4 mm. This spacer is manually introduced just for the set-up of the machine and is removed afterwards. The height of the spacer is the difference between the pretended height and the 2 mm limit.

The array is fabricated out of a [100] p-type boron-doped silicon wafer with $1.3\ \text{m}\Omega\cdot\text{cm}$ resistivity and a thickness of 5 mm (figure 2(a)). The fabrication process starts by making a set of 1.5 mm deep cuts on the backside of the silicon substrate to create squared pad regions with dimensions of $0.45 \times 0.45 \times 1.5\ \text{mm}^3$ (figure 2(b)). The pad regions represent the electrical contacts of each electrode in the array. The next step consists of filling the grooves with a non-conductive epoxy resin (Loctite® Hysol 9492) in order to electrically isolate each electrode from its neighbours (figure 2(c)). The epoxy excess is removed through grinding and polishing. After cutting the electrode shafts, the epoxy resin is used to cluster all shafts in a single structure.

Afterwards, the front side of the silicon substrate is diced to produce three steps with different heights. This is accomplished by multiple closely-spaced dicing cuts, in order to remove all the silicon between cuts. Each of these closely-spaced cuts produces a step that is 0.5 mm shorter than the

previous one. Thus, the set of cuts for the higher shafts are performed at the substrate's surface, followed by a set of cuts 0.5 mm deeper and so on, as shown in figure 2(d). The next step consists of the shaft's formation, which results in a 6×6 matrix. Two sets of deep orthogonal cuts are made on the upper side of the silicon substrate. The backside pads that are initially 1.5 mm deep are reduced at this step to a thickness of 0.5 mm, connected by a 0.15 mm wide layer of epoxy 9492. The result of this dicing step is $36 \times 0.15 \times 0.15\ \text{mm}^2$ wide shafts with penetrating depths of 3 mm, 3.5 mm and 4 mm (figure 2(e)). This technology also allows other combinations of shaft lengths, suitable for other applications.

After the shafts are properly shaped and electrically insulated from each other, it is necessary to encapsulate the array. This is accomplished by placing the array into a square mold filled with a medical epoxy adhesive (Loctite® M-31CL™), which after curing will result in a complete covering of the array with a biocompatible resin [30] (figure 2(f)). The pad regions provide electrical access to each shaft, so the medical epoxy layer in the array's backside is removed through grinding and polishing.

In order to smooth the process of the electrodes' implantation into the neural tissue, sharpening of the shaft tips is performed. Since the blunt shafts comprise different lengths, this step has to be completed once again at increasing depths with an index of 0.5 mm between cuts. Therefore, graded and sharpened shafts are produced, as shown in figure 2(g). This dicing step is accomplished by a V-shape $250\ \mu\text{m}$ thick Disco Z09 blade that makes a 60° angle with the surface. The cutting speed is $0.5\ \text{mm s}^{-1}$. The sharp tips formation is accomplished at this step so the area of the transduction layer can be properly controlled, exposing only the sharp tips of the shafts.

The next step is the deposition of the transduction layer in order to convert the silicon shafts into active electrodes for recording or stimulation (figure 2(h)). The transduction layer consists of 50 nm of Ti and 200 nm of Pt layers. The Pt layer will allow an efficient charge transfer between the electrode and the neural tissue while Ti serves as an adhesive layer. The Ti layer was deposited using electron beam evaporation at a

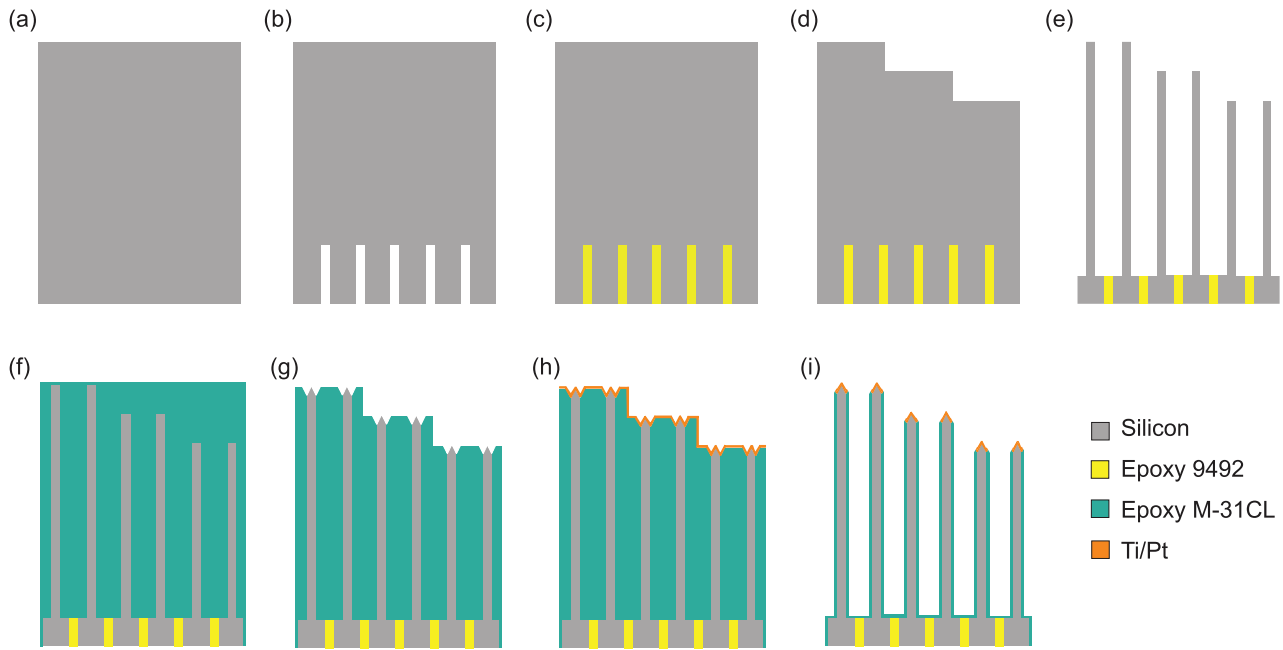


Figure 2. Cross-sectional drawings of the fabrication steps. (a) Silicon substrate; (b) pads' region fabrication; (c) adhesive filling with epoxy 9492 resin; (d) silicon steps produced by closely-spaced cuts; (e) blunt shafts with lengths of 4 mm (left), 3.5 mm (centre) and 3 mm (right), spaced 0.6 mm apart; (f) array's encapsulation by medical epoxy M-31CL resin; (g) diced sharp shaft tips at different depths; (h) deposition of Ti/Pt layers; (i) medical epoxy removal by dicing.

starting pressure of 8.6×10^{-6} mBar while supplying a current of 8 mA and a potential of 7 kV. The duration of the deposition was 2 min (deposition rate approximately 5 \AA s^{-1}) and the maximum temperature measured at the substrate was 60 °C. The Pt layer was deposited using DC sputtering at a starting pressure of 1×10^{-2} mBar while supplying a 40 sccm of Argon, a current of 40 mA and a potential of 302 V. The duration of the deposition was 251 min (deposition rate approximately 0.15 \AA s^{-1}) and the maximum temperature measured at the substrate was 37 °C. Both depositions are performed in the same vacuum environment, so that the Pt layers are deposited over the Ti layers before they are exposed to the atmosphere.

The final 3D array is accomplished by removing the excess of the medical epoxy. Once again two sets of deep orthogonal cuts are made on the upper side of the silicon substrate, leaving each shaft with a thin layer of medical epoxy (figure 2(i)). The result of this dicing step is thirty-six $180 \times 180 \mu\text{m}^2$ wide shafts with penetrating depths of 3 mm, 3.5 mm and 4 mm.

4. Results

4.1. Fabrication process

The results of the 3D MEA fabrication are shown in figure 3, which comprises transversal and 3D views of each fabrication step. All photos and measurements were performed with a Leica M80™ stereo microscope and Leica LAS™ software. Figure 3(a) shows the thick silicon substrate which undergoes a dicing process to create the 3D MEA. The dicing step result to create the electrical contact pads is shown in figure 3(b) at multiple views. The initial pad regions are $0.45 \times 0.45 \pm 0.013 \text{ mm}^2$ wide and 1.5 ± 0.027 mm deep.

The result of filling the grooves with epoxy resin is shown in figure 3(c). In figure 3(d) one can see the staircase effect on the upper side of the silicon substrate, in order to produce flat shafts. The shafts created are 4 ± 0.017 mm, 3.5 ± 0.009 mm and 3 ± 0.014 mm deep and 0.15 ± 0.005 mm wide as shown in figure 3(e). At this stage, the final contact pad lengths are set to 0.5 ± 0.043 mm. The results of the insulation process are shown in figure 3(f) and one can see that the total shaft area is encapsulated by the medical epoxy layer. In figure 3(g), the result of dicing the sharp tips is shown. Figure 4 shows the array's shafts with the sharp tips, which have lengths of 0.15 ± 0.006 mm and a radius tip of $2.41 \mu\text{m}$. The tip measurement was performed in a FEI Nova NanoSem™ 200. The final 3D MEA can be seen in figure 3(h).

A 6×6 matrix of electrodes with different penetrating depths spacing each electrode by $600 \mu\text{m}$ and insulated by a $15 \pm 3.6 \mu\text{m}$ layer of a medical epoxy resin was successfully produced. The final characteristics of the array are summarized in table 2. During the final cutting step, only the shaft's body undergoes a dicing process. Thus, Ti/Pt transduction layers on the shaft's tips are able to withstand this step. Although we have presented a detailed process flow with a single array sample, the proposed 3D arrays are compatible with a batch-scale fabrication process.

4.2. Mechanical characterization

The 3D MEA robustness was characterized by measuring the compressive failure forces of the shafts and the array's bending force. We also measured the load required to implant and extract the array into a substrate of 0.5% agar gel and a porcine cadaver brain. A total of five porcine cadaver brain

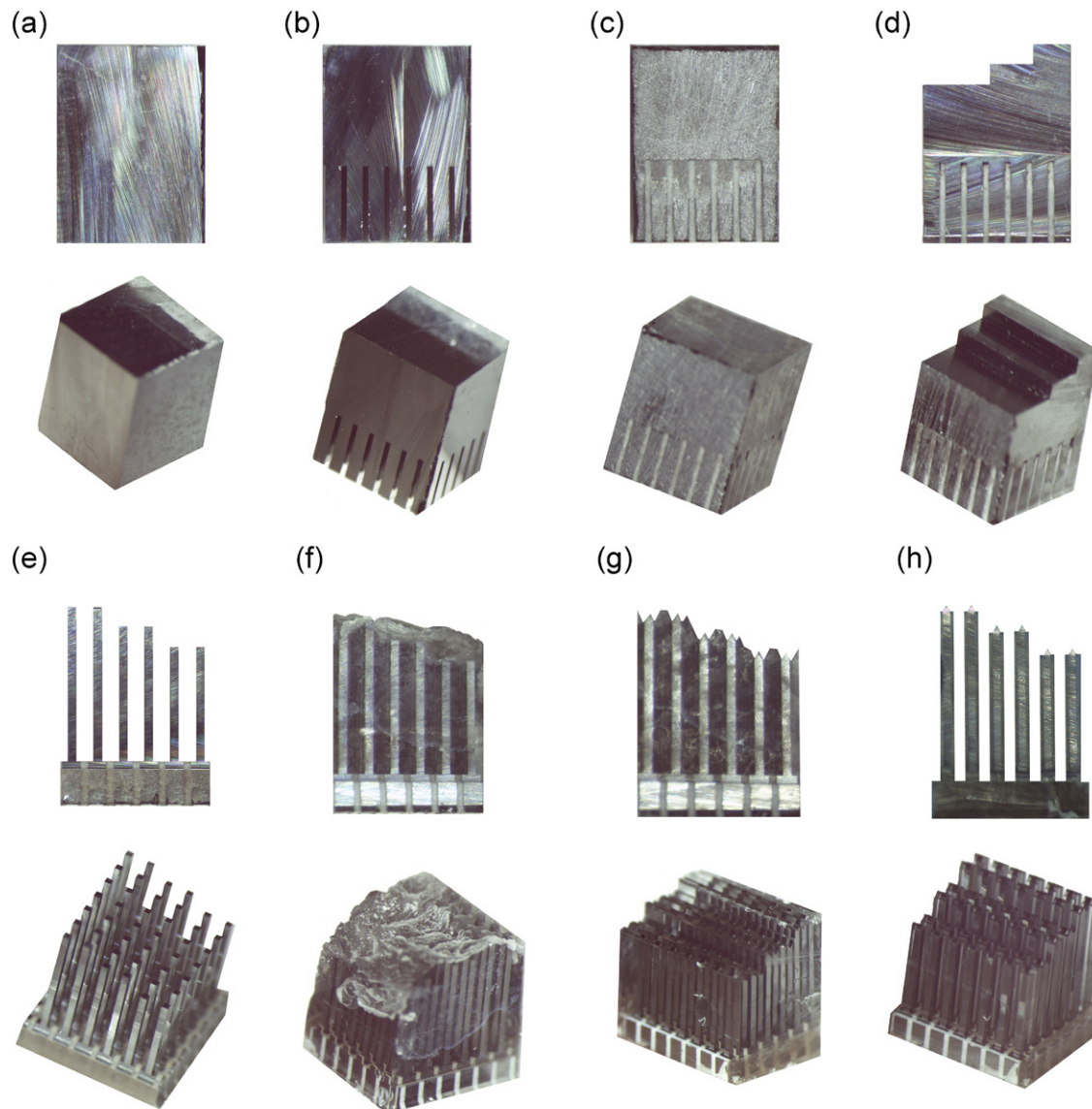


Figure 3. Transversal (top) and 3D photos (bottom) of the array fabrication steps. (a) Silicon substrate; (b) diced contact pads; (c) filling with epoxy 9492 resin; (d) diced substrate's upper side to produce three steps; (e) diced blunt shafts with lengths of 4 mm (left), 3.5 mm (center) and 3 mm (right), spaced 0.6 mm apart; (f) array's insulation by medical epoxy resin; (g) diced sharp shaft tips at different depths; (h) medical epoxy removal by dicing, producing a 6 × 6 matrix of electrodes.

samples were used. They were conserved at $-18\text{ }^{\circ}\text{C}$ for 12 h and 30 min before the mechanical tests they were preserved at $5\text{ }^{\circ}\text{C}$. During the tests, both gel and brain tissue were exposed to the room temperature.

The tests were performed on a Shimadzu AG-IS dynamometer equipped with a 50 N load cell capable of a 5 mN resolution. For the longitudinal compressive failure force tests, due to the high forces involved a 500 N load cell with 50 mN resolution was used. The implantation and withdrawal tests include three different speeds. Only 4 mm shafts composed the tested 6 × 6 arrays in order to represent the worst case scenario.

The array's mechanical characterization focused on its robustness. The electrodes' compressive failure forces were measured as well as the array's base bending force. The setup photo and load versus displacement graphic results are shown

in figure 5. In longitudinal compression tests (figure 5(a)), the shafts withstand a load of approximately $68.37 \pm 8.63\text{ N}$ before breakage. Figure 5(b) shows the axial compression failure tests on single shafts. The array is horizontally placed in a support made of aluminum with a 15 mm spacing between support points. An aluminum block made a downward displacement until it reaches the shaft at 2/3 of its height. The results show that up to 60 mN is required to break a single shaft. In order to measure the array's base bending force, a three point flexural test was used. The tested sample was 19.2 mm wide and 4 mm long (figure 5(c)). A downward force was applied in the middle of the sample with a cylindrical aluminum support until sample rupture could be observed. A maximum deflection before a rupture of 0.3 mm was achieved with a required load of 1.8 N.

We also measured the array's insertion and withdrawal forces (10 separate samples for each test) into two different

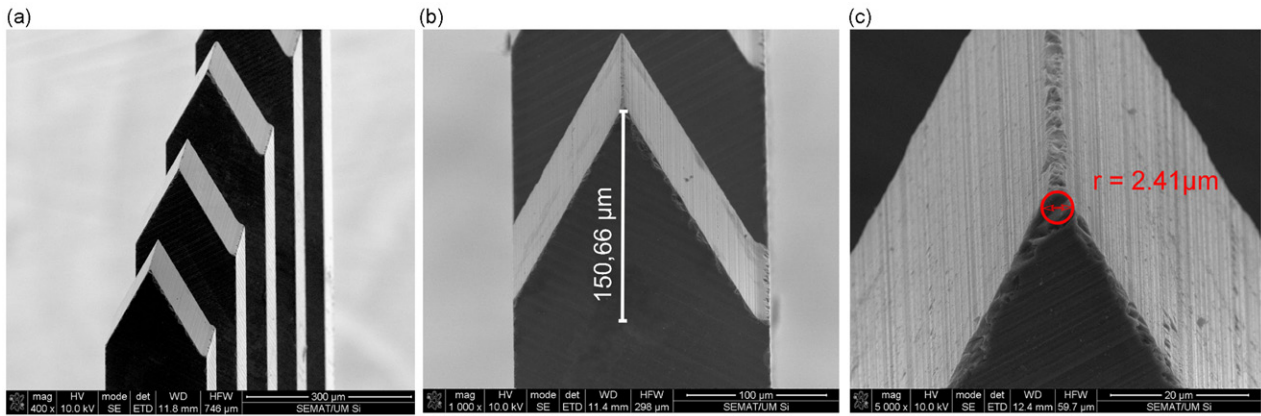


Figure 4. SEM images of (a) the array’s sharp shafts, (b) the tip’s height of approximately 150 μm and (c) the radius tip of 2.41 μm.

Table 2. Summary of geometrical properties of the fabricated 3D probes arrays.

Array’s dimensions	3.45 × 3.45 mm ²	Shaft width	180 μm
Contact pad width	0.45 × 0.45 mm ²	Shaft length	3, 3.5 and 4 mm
Contact pad height	500 μm	Tip length	150 μm
Space between shafts	600 μm	Tip radius	2.41 μm

substrates: 0.5% agar gel and a porcine cadaver brain. Agar gel was used as an in vitro alternative for brain tissue [31, 32]. Figures 6(a) and (d) demonstrates the setup arrangement for the implantation analysis on agar and brain tissue, respectively. The array was attached to the dynamometer shaft (positioned perpendicular to the substrate surface), which moved downward towards the substrate at a predetermined speed. After penetration, the dynamometer shaft paused for 30 s before initiating the withdrawal tests, where the probe returned to its initial position, removing it from the tissue. The shaft was set to move at three different speeds, namely, 180 mm min⁻¹, 120 mm min⁻¹ and 50 mm min⁻¹. The surfaces of the substrates were determined by manually lowering the array until a small force was registered on the load cell. The array was then raised slightly just until the load on the probe returned to zero.

Figures 6(b) and (e) shows the force applied versus the array’s displacement towards the gel and brain, respectively. Each figure shows the key moment highlighted by a number. In both insertion tests, we observed an increase in the force applied on the initial stage while the array is still subjected to the gel or brain’s resistance until the moment where the electrode tips pierce the surface. Beyond this moment, as expected, there was an abrupt drop in the required load, which corresponds to moment 1, identified in the figures. After the electrode’s full penetration there was a slight increase in the curve’s slope, indicating that the array’s base was pushing against the gel or brain’s surface (moment 2). The withdrawal test results on agar and the brain are shown in figures 6(c) and (f), respectively. In moment 3 there is a maximum tension

applied until a complete detachment between the array and the tested material is accomplished (moment 4). The rise in tension during withdrawal is due to the drag forces between the electrodes and the surrounding material. Table 3 summarizes the acquired data on the implantation and withdrawal tests.

4.3. Electrochemical characterization

In vitro electrochemical impedance spectroscopy (EIS) was used to perform electrochemical characterization. The surface area of the Pt films was 0.02 mm². The impedance measurements were performed in a Gamry system (Gamry Instruments, Reference 600™), using a standard three-electrode configuration. A large-area platinum foil (40 × 40 × 0.25 mm³) was used as a counter electrode and an Ag|AgCl reference electrode. The electrolyte employed was a 0.9% NaCl solution. Impedance (Z) was measured for frequencies from 1 Hz to 1 MHz at a constant 10 mV AC voltage. All measurements were made at room temperature.

At 1 kHz, in vitro EIS measurements showed an average impedance of 68 kΩ for Pt thin-films. The impedance at this specific frequency is of neurobiological interest because the neuronal cell’s action potential has a duration close to 1 ms and therefore, provides the attenuation introduced by the electrode for this range of frequencies. Figure 7(a) shows the Bode plot of the impedance magnitude versus frequency for the sputtered Pt thin-film. Three readings of the same sample were performed for increased measurement reliability. The electrode exhibits a capacitive behaviour in all the frequency ranges (figure 7(b)).

5. Discussion and conclusion

This paper proposed a different fabrication method of 3D silicon-based neural MEA with long electrodes of different penetrating depths. The 3D arrays were patterned relying only on dicing saw technology and successfully producing a matrix of 6 × 6 electrodes. Arrays of up to 4 mm long, 180 μm wide and individually addressable were fabricated. The described fabrication process is simple, reproducible and robust enough for batch fabrication.

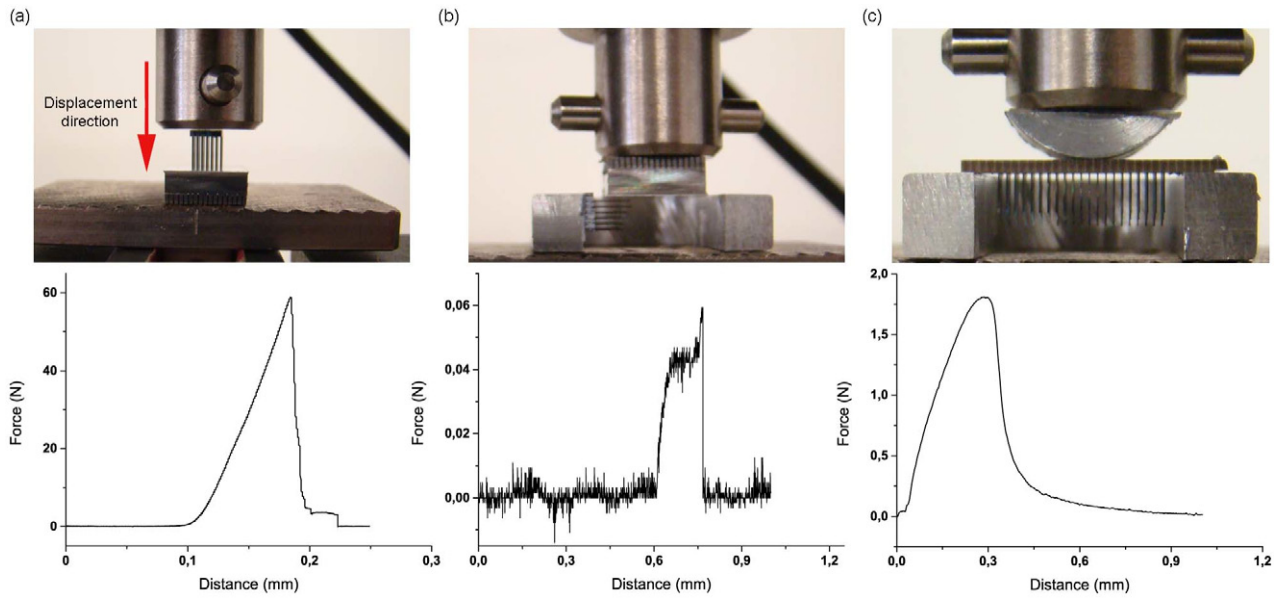


Figure 5. Mechanical failure tests. The first row of photos corresponds to the setup arrangement and the second row to the force versus displacement graphic for the three tests. (a) Longitudinal and (b) axial compressive force and (c) bending force.

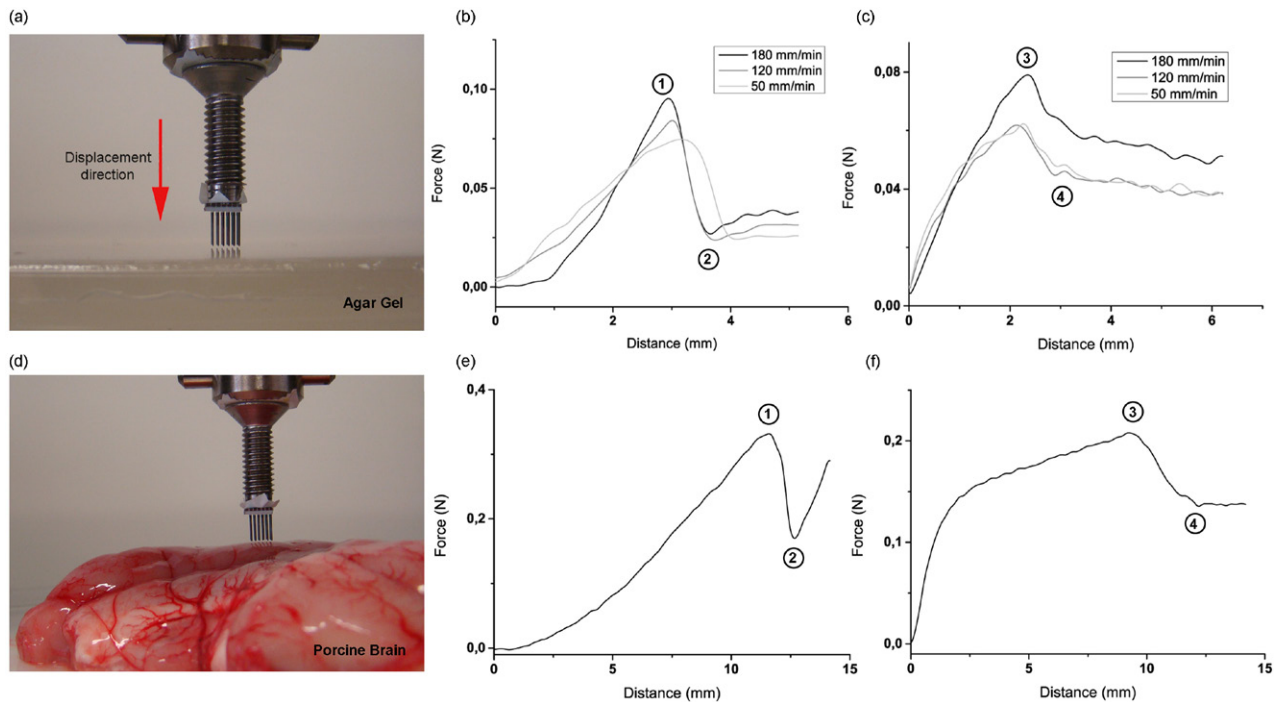


Figure 6. Experimental setup photo used in the mechanical tests on (a) 0.5% agar gel. Displacement versus force graphic for the (b) insertion and (c) removal tests on agar gel at different speeds. (d) Setup photo for the tests on the porcine cadaver brain. Displacement versus force graphic for the (e) insertion and (f) removal tests on the porcine brain at a velocity of 180 mm min^{-1} .

Wang *et al* [25] presented a self-assembled array probe based on silicon wet-etching micromachining to produce the array design and use heat treatment processes to achieve the final probe. Although it creates shafts 4 mm deep, this technology is limited to the number of shafts in the array (see table 1). Rakwal *et al* [24] introduced a fabrication process (μ -WEDM) capable of producing a 10×10 array with shaft lengths up to 9 mm. Although this sounds like a promising method, it is not standard industry technology. On the other

hand, the fabrication process used in this paper employs standard micromachining technology. Moreover, the reported sharp tips have been realised through silicon etching processes [33, 34]. The proposed fabrication method avoids etching processes, producing the sharpened shaft tips with a set of dicing cuts using a V-shaped blade.

The final 3D probe also comprises different shaft lengths: 4, 3.5 and 3 mm. This technology is compatible with different lengths and also a superior number of different shaft heights

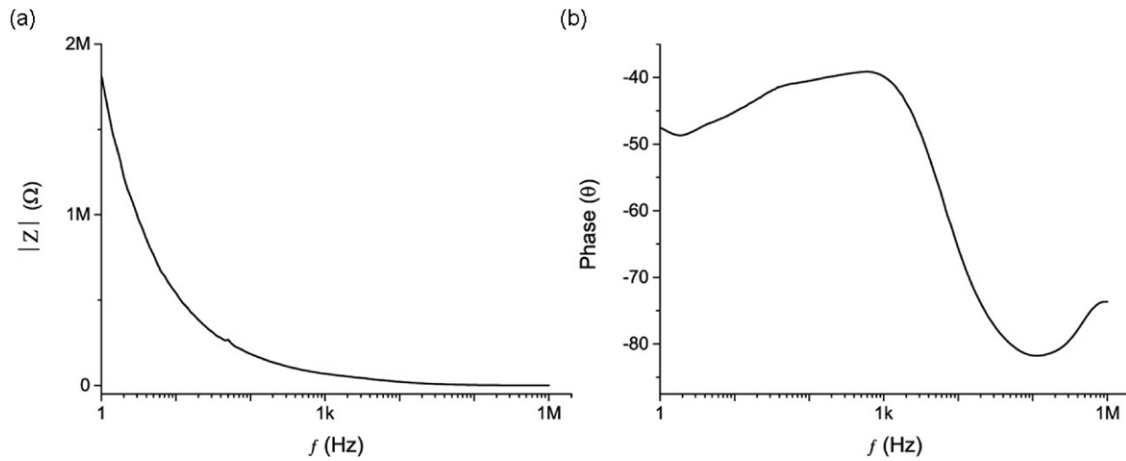


Figure 7. Bode plot of the EIS tests in saline solution: (a) magnitude; (b) phase angle.

Table 3. Statistical data of the implantation and withdrawal tests. The number of samples was 10 for each test. The presented values correspond to the average maximum force measured in each test.

Material	Speed (mm min ⁻¹)	Implantation force (mN)	Force per electrode (mN)	Withdraw force (mN)	Force per electrode (mN)
0.5% Agar Gel	50	87.04 ± 8.93	2.42	68.6 ± 7.58	1.91
	120	94.75 ± 31.37	2.63	68.57 ± 9.49	1.93
	180	95.45 ± 14.49	2.65	74.23 ± 8.25	2.06
Porcine brain	180	444.54 ± 90.37	12.5	250.53 ± 30.54	6.96

that may be changed depending on the desired application. Probes with different penetrating depths allow us to reach a wider spatial region and decrease the number of redundant electrodes, providing a more selective recording and stimulating of the neural tissue. For *in vivo* applications, the brain’s opening required to implant the proposed MEA is defined by the backside end of the array, which is approximately 3.45 × 3.45 × mm². This are more favourable results compared to the reported compact array, with opening areas of 5.7 × 4 mm² [19] and 5 × 5 mm² [21].

The mechanical characterization shows a robust MEA. Results showed that the longer shafts withstand a longitudinal compressive load of approximately 68 N before the electrodes break and it requires a 1.8 N load before the array’s base rupture. The electrodes are more fragile when an axial compression is applied, breaking with a 60 mN load. Nevertheless, the insertion force required to penetrate the brain reported in literature is of the order of several mN [28, 35, 36], which indicates that these MEA are strong enough to withstand the forces required at implantation time.

Many designs of long probes fail (crack or shatter) during implantation as they are unable to withstand the insertion axial forces, retraction forces and tension forces of the brain tissue [37]. Thus, the array’s insertion and withdrawal forces have been quantified using a brain cortex phantom (0.5% agar gel) and a porcine cadaver brain. In both the agar gel and brain tissue, none of the tested samples showed any sign of shaft breakage during and after the mechanical tests.

In the agar tests different penetration and withdrawal speeds were applied. Although average load values seemed to increase along with the increased speed of the test, the

large standard deviation values (especially at 120 mm min⁻¹) do not allow it to reach a correlation between the increased speed and load. However, low insertion speeds are expected to result in lower required loads, since they have the advantage of generating minimal vibration and mechanical shock to the tissue inserted while inserting electrodes, allowing the implantation surface to accommodate the probe more successfully [28, 35]. Also, as expected, higher loads are consistently required to pierce the arrays into the substrates than to withdraw them, since the only force involved in withdrawing tests are the drag forces between the electrodes and the surrounding material. However, by comparing agar and brain tissue results, we can conclude that the insertion and withdrawal results are highly dependent on the insertion material. This is because agar gel phantoms do not incorporate the heterogeneous composition of neural tissue, which will have considerable impact on the dynamics of insertion and tissue deformation. Brain tissue insertion tests performed at a lower speed (50 mm min⁻¹ and 120 mm min⁻¹) showed significant tissue dimpling without implantation success. High speed insertion tests (180 mm min⁻¹) were successful, resulting in maximum forces with a magnitude six times higher than with agar to penetrate the electrodes. This difference in magnitude can be explained by the required force to pierce the brain’s dura matter layer.

Jensen *et al* [35] demonstrated that the insertion forces increase with the number of shafts within the array. Thus, the results obtained are consistent with those reported in the order of several mN, higher in magnitude due to the increased number of shafts (36 electrodes). In both agar and brain tissue, the required insertion and withdrawal forces per electrode are

within this range. The results on the agar gel and the brain's maximum force per electrode are in the same of magnitude obtained by Das *et al* [32]. Other studies [28, 36] have been performed in order to measure the insertion forces in a rat's brain, obtaining lower magnitudes of force than those obtained in this paper. These results were achieved due to the fact that the dura matter were removed previous to the insertion test and only pia matter had to be penetrated at implantation time.

Overall, the proposed design and fabrication procedure is an eligible alternative for long 3D MEA technology that allows neural signal recording and stimulation. It also offers a contribution to future studies addressing the importance of additional insertion parameters for optimal device insertion.

Acknowledgments

ACP is supported by the Portuguese Foundation for Science and Technology (SFRH/BD/89509/2012). This work was also supported by FCT with the project reference FCOMP-01-0124-FEDER-010909 (FCT/PTDC/SAU-BEB/100392/2008).

References

- [1] Perlmutter J and Mink J 2006 *Annu. Rev. Neurosci.* **29** 229–57
- [2] Mogilner A, Benadib A and Rezaei A 2001 *Thalamus Relat. Syst.* **1** 255–67
- [3] Wilson B and Dorman M 2008 *Hearing Res.* **242** 3–21
- [4] Yanai D, Weiland J, Mahadevappa M, Greenberg R, Fine I and Humayun M 2007 *Am. J. Ophthalmol.* **143** 820–7
- [5] Collinger J, Wodlinger B, Downey J, Wang W, Tyler-Kabara E, Weber D, McMorland A, Velliste M, Boninger M and Schwartz A 2013 *Lancet* **381** 557–64
- [6] Hochberg L, Serruya M, Friehs G, Mukand J, Saleh M, Caplan A, Branner A, Chen D, Penn R and Donoghue J 2006 *Nature* **442** 164–71
- [7] Chang C and Chiou J 2010 *Sensors* **10** 4238–52
- [8] Ruther P, Herwik S, Kisban S and Seidl K 2010 *IEEE Trans. Electr. Electron. Eng.* **5** 505–15
- [9] Normann R A 2007 *Nat. Rev. Neurol.* **3** 444–52
- [10] Wise K 2005 *IEEE Eng. Med. Biol. Mag.* **24** 22–9
- [11] Bhandari R, Negi S, Rieth L, Normann R and Solzbacher F 2009 *J. Micromech. Microeng.* **19** 035004
- [12] Song Y *et al* 2005 *IEEE Trans. Neural Syst. Rehabil. Eng.* **13** 220–6
- [13] Wark H *et al* 2013 *J. Neural Eng.* **10** 045003
- [14] Hajj-Hassan M, Chodavarapu V and Musallam S 2009 *Micro Nano Lett.* **4** 53–8
- [15] Kindlundh M, Norlin P and Hofmann U 2004 *Sensors Actuators B* **102** 51–8
- [16] Seidl K, Herwik S, Torfs T, Neves H, Paul O and Ruther P 2011 *J. Microelectromech. Syst.* **20** 1439–48
- [17] Bai Q, Wise K and Anderson D 2000 *IEEE Trans. Biomed. Eng.* **47** 281–9
- [18] Bai Q and Wise K 2001 *IEEE Trans. Biomed. Eng.* **48** 911–20
- [19] Yao Y, Gulari M, Wiler J and Wise K 2007 *J. Microelectromech. Syst.* **16** 977–88
- [20] Du J, Roukes M and Masmanidis S 2009 *J. Micromech. Microeng.* **19** 075008
- [21] Herwik S *et al* 2009 *J. Micromech. Microeng.* **19** 074008
- [22] Perlin G and Wise K 2010 *J. Microelectromech. Syst.* **19** 1409–21
- [23] Jones K, Campbell P and Normann R 1992 *Ann. Biomed. Eng.* **20** 423–37
- [24] Rakwal D, Heamawatanachai S, Tathireddy P, Solzbacher F and Bamberg E 2009 *Microsyst. Technol.* **15** 789–97
- [25] Wang M, Maleki T and Ziaie B 2010 *J. Micromech. Microeng.* **20** 035013
- [26] Peixoto A, Goncalves S, Silva A, Dias N and Correia H 2013 *IEEE Sensors J.* **13** 3319–24
- [27] Kjonigsen L, Leergaard T, Witter M and Bjaalie J 2011 *Front. Neuroinform.* **5** 2
- [28] Paralikar K and Clement R 2008 *IEEE Trans. Biomed. Eng.* **55** 2258–67
- [29] Boretius T, Jurzinsky T, Koehler C and Kerzenmacher S 2011 *Conf. Proc. IEEE Engineering in Medicine and Biology Society* pp 5404–7
- [30] Henkel A G & Co. 2005 Loctite® M-31CL™ Technical Data Sheet Available: www.henkel.co.uk/2838_UKE_HTML.htm?nodeid=8797726048257
- [31] Pomfret R, Miranpuri G and Sillay K 2013 *Ann. Neurosci.* **20** 118–22
- [32] Das R, Ghandi D, Krishnan S, Saggere L and Rousche P 2007 *IEEE Trans. Biomed. Eng.* **54** 1089–96
- [33] Wu J, Feng W, Tang W and Zeng F 2006 *Conf. Proc. IEEE Engineering in Medicine and Biology Society* pp 3166–9
- [34] Bhandari R, Negi S, Rieth L, Normann R and Solzbacher F 2008 *Sensors Actuators A* **145–6** 123–30
- [35] Jensen W, Yoshida K and Hofmann U 2006 *IEEE Trans. Biomed. Eng.* **53** 934–40
- [36] Sharp A, Ortega A, Restrepo D, Curran-Everett D and Gall K 2009 *IEEE Trans. Biomed. Eng.* **56** 45–53
- [37] Hajj-Hassan M, Chodavarapu V and Musallam S 2008 *Sensors* **8** 6704–26